PERGAMON International Journal of Mechanical Sciences 43 (2001) 1483–1506

International Journal of MECHANICAL SCIENCES

www.elsevier.com/locate/ijmecsci

The plastic collapse of sandwich beams with a metallic foam core

C. Chen, A-M Harte, N.A. Fleck*

Department of Engineering, University of Cambridge, Trumpington Street, Cambridge, CB2 1PZ, UK

Received 7 April 2000

Abstract

Plastic collapse modes of sandwich beams have been investigated experimentally and theoretically for the case of an aluminium alloy foam with cold-worked aluminium face sheets. Plastic collapse is by three competing mechanisms: face yield, indentation and core shear, with the active mechanism depending upon the choice of geometry and material properties. The collapse loads, as predicted by simple upper bound solutions for a rigid, ideally plastic beam, and by more refined finite element calculations are generally in good agreement with the measured strengths. However, a thickness effect of the foam core on the collapse strength is observed for collapse by core shear: the shear strength of the core increases with diminishing core thickness in relation to the cell size. Limit load solutions are used to construct collapse maps, with the beam geometrical parameters as axes. Upon displaying the collapse load for each collapse mechanism, the regimes of dominance of each mechanism and the associate mass of the beam are determined. The map is then used in optimal design by minimising the beam weight for a given structural load index.

Keywords: Plastic collapse; Sandwich beam; Metal foam; Minimum weight

1. Introduction

Recently, a range of metallic foams have been developed with a relative density $\hat{\rho}$ (defined by the ratio of foam density to the density of the cell walls) in the range 0.05–0.3. Mostly, they are based on aluminium alloys, although steel foams and creep-resistant nickel alloy foams are also under development. The interested reader is referred to Ashby et al. [1] for a comprehensive review of the

* Corresponding author. Tel.: + 44-01223-332650; fax: + 44-01223-332662.
E-mail address: naf1@eng.cam.ac.uk (N.A. Fleck).

0020-7403/01/$ - see front matter
PII: S0020-7403(00)00069-2

manufacture, properties and uses of these new materials. Metallic foams compete favourably with polymer foams as the lightweight cores of sandwich beams, plates and shells, due to the higher stiffness and high-temperature capability. Clearly, it is important to determine the sensitivity of the collapse strength and failure mode to the structural geometry and to the properties of the constituent materials.

In this study, sandwich beams have been manufactured with an Alporas[1] aluminium alloy foam core, and cold-rolled aluminium face sheets in the half-hard condition. The monotonic collapse response of the beams has been measured for a wide range of geometries, under four-point bend loading. Four-point bend loading allows the competing failure modes of face yield, core shear and indentation to be separated physically along the beam: face yield occurs between the inner rollers, core shear occurs between the inner and outer rollers and indentation is triggered directly beneath the rollers. The measured load–deflection behaviour of the sandwich beams are compared with limit load formulae for rigid, ideally plastic beams and with more refined finite element calculations. Collapse mechanism maps, with the geometrical parameters of the beam as axes, are generated using the limit load formulae, and minimum weight designs are obtained as a function of an appropriate structural load index. The current study has been performed in parallel with those of Bart-Smith et al. [2], and McCormack et al. [3]: they considered the three-point bend loading of sandwich beams by flat indenters.

2. Prediction of the behaviour of sandwich beams in four-point bending

We begin by summarising analytical formulae for the stiffness and collapse strength of sandwich beams in four-point bending, assuming both core and face sheets are elastic-ideally plastic isotropic solids. Then, in Section 2.2, a finite element method is outlined in order to obtain a more accurate prediction of the collapse response; for such purposes, the measured elastic–plastic responses of the face sheets and core are employed.

2.1. Analytical formulae for the stiffness and strength

Consider a sandwich beam of uniform width b, comprising two identical face-sheets of thickness t perfectly bonded to a metallic foam core of thickness c. The beam is loaded in four-point bending by circular cylindrical rollers of radius R, and each roller carries a load of $F/2$ as sketched in Fig. 1. The span between the outer supports is ℓ; the overhang distance beyond the outer supports is H; and the two inner indenters are spaced a distance s apart. Both the core and face-sheets are treated as isotropic, elastic-ideally plastic solids, with a Young's modulus E_f for the face-sheet and E_c for the core.

The relative elastic deflection δ of inner and outer rollers is the sum of the flexural and shear deflections (see Ref. [4]),

$$\delta = \frac{F(\ell - s)^2(\ell + 2s)}{48(EI)_{eq}} + \frac{F(\ell - s)}{4(AG)_{eq}}, \tag{1}$$

[1] European supplier, Karl Bula, Innovation Services, Ch-5200 Brugg, Herrenmatt 7F, Switzerland.

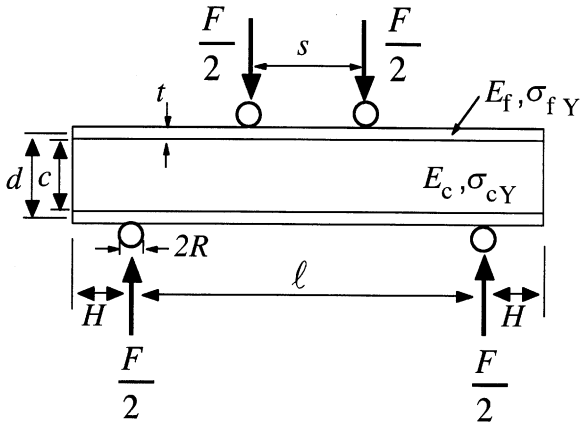

Fig. 1. A sandwich beam under four-point loading.

where the equivalent flexural rigidity $(EI)_{eq}$ is

$$(EI)_{eq} = \frac{E_f btd^2}{2} + \frac{E_f bt^3}{6} + \frac{E_c bc^3}{12} \approx \frac{E_f btd^2}{2} \tag{2}$$

and $(AG)_{eq}$, the equivalent shear rigidity, is

$$(AG)_{eq} = \frac{bd^2}{c} G_c \approx bcG_c \tag{3}$$

in terms of the shear modulus G_c of the core, the cross-sectional area A of the core, and the spacing $d = c + t$ of the mid-planes of the face-sheets.

In the design of sandwich beams it is usually necessary to evaluate the collapse strength in addition to the stiffness of candidate beams. Upper bound calculations of competing collapse modes can be used to derive simple analytical formulae; for this purpose the foam core and solid face-sheets are treated as rigid, ideally plastic solids of uniaxial strength σ_{fY} and σ_{cY}, respectively. The following derivations are summarised from a more complete treatment given by Ashby et al. [1].

2.1.1. Face yield

Sandwich beams with low yield strength face sheets collapse at a limit load F_{FY} set by face yield. The simplest approach is to assume that plastic collapse occurs when the face sheets attain the yield strength σ_{fY} while the core yields simultaneously at a stress level of σ_{cY}. The collapse load is determined by equating the maximum bending moment within the sandwich beam to the plastic collapse moment of the section, giving

$$F_{FY} = \frac{4bt(c+t)}{\ell - s}\sigma_{fY} + \frac{bc^2}{\ell - s}\sigma_{cY}. \tag{4}$$

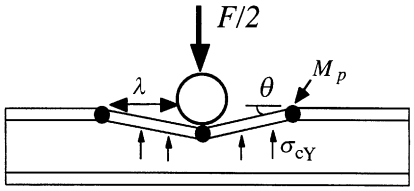

Fig. 2. Indentation mode for a sandwich beam.

This relation can be simplified by neglecting the contribution of the core to the plastic collapse moment, as given by the second term on the right-hand side of Eq. (4).

2.1.2. Indentation

The indentation mode of collapse involves the formation of three plastic hinges within the top face sheet adjacent to each indenter, with compressive yield of the underlying core, as sketched in Fig. 2. Early studies on the indentation of polymer foams (for example, Ref. [5]) and more recently on metal foams [6] reveal that the indentation pressure is only slightly elevated above the uniaxial compressive strength, due to the compressibility of the foam [7].

The collapse load $F/2$ on each roller can be derived by a simple upper bound calculation, wherein two segments of the upper face, of wavelength λ, are rotated through a small angle θ. The resulting collapse load is given by

$$F = \frac{8M_p}{\lambda} + 2\lambda b\sigma_{cY}, \tag{5}$$

where $M_p = \sigma_{fY} bt^2/4$ is the full plastic moment of the face-sheet section. Minimisation of this upper bound solution for F with respect to the free parameter λ gives an indentation load F_I of

$$F_I = 4bt\sqrt{\sigma_{cY}\sigma_{fY}} \tag{6}$$

and a wavelength

$$\lambda = t\sqrt{\frac{\sigma_{fY}}{\sigma_{cY}}}. \tag{7}$$

We note in passing that the same expressions for P_I and λ as given by Eqs. (6) and (7) are obtained by a lower bound calculation, by considering equilibrium of the face sheet and yield of the face sheet and core. The details are given by Ashby et al. [1]. We conclude that these bounds give exact values for the collapse load, and for the span length λ between plastic hinges. A word of caution, however. The upper and lower bound analyses are based on beam theory, which is an approximation. Thus, the beam theory solution may be greater than or less than the collapse loads as predicted by more refined methods (such as the finite element method) or by experiment.

2.1.3. Core shear

When a sandwich panel is subjected to a transverse shear force the shear force is carried mainly by the core, and plastic collapse by core shear can result. Two competing collapse mechanisms can

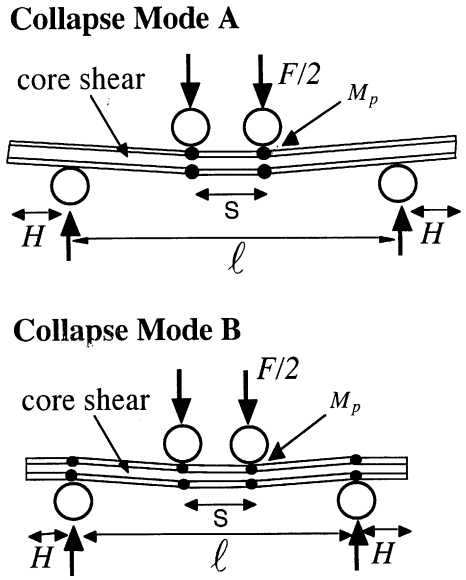

Fig. 3. Competing collapse modes A and B for core shear of a sandwich beam in four-point bending.

be identified, as shown in Fig. 3: Mode A comprises the formation of plastic hinges in the face sheets beneath the inner rollers whilst Mode B consists of plastic hinges in the face sheets adjacent to all rollers. For both Modes A and B the core yields in shear.

Consider first collapse Mode A (see Fig. 3). A simple work calculation can be performed to calculate the collapse load F_A by assuming the face sheets on the right side of the sandwich panel rotates through an angle θ whereas the left side rotates through an angle $-\theta$. Consequently, the foam core shears by an angle $-\theta$. On equating the external work done $F(\ell - s)\theta/2$ to the internal work dissipated within the core of length $(\ell + 2H - s)$ and at the four plastic hinges in the face sheets, we obtain

$$F_A = 2\frac{bt^2}{\ell - s}\sigma_{fY} + 2bc\tau_{cY}\left(1 + \frac{2H}{\ell - s}\right), \tag{8}$$

where τ_{cY} is the shear yield strength for the foam core. Typically, the shear strength of a foam is about two-thirds of the uniaxial strength, $\tau_{cY} \approx 2\sigma_{cY}/3$. We note from Eq. (8) that F_A increases linearly with the length of overhang H beyond the outer supports.

Second, consider collapse Mode B. As sketched in Fig. 3, this collapse mechanism involves the formation of plastic hinges in the face sheets at both inner and outer supports. The core undergoes simple shear over the length $(\ell - s)$ between the outer supports, with no deformation beyond the outer supports. A work calculation gives for the plastic collapse load F_B,

$$F_B = 4\frac{bt^2}{\ell - s}\sigma_{fY} + 2bc\tau_{cY}. \tag{9}$$

Since the two calculations given above are upper bound calculations of the actual collapse load, the lower of the two collapse loads is taken as an estimate for the actual collapse load. Collapse Mode A is activated for small lengths of overhang whereas collapse Mode B has a lower collapse load for large overhangs. The transition length of overhang H_t is determined by equating Eqs. (8) and (9), giving

$$H_t = \frac{1}{2}\frac{t^2}{c}\frac{\sigma_{fY}}{\tau_{cY}}. \tag{10}$$

In order to gauge the practical significance of the overhang, let us take some representative values for a typical sandwich panel comprising aluminium skins and a metallic foam core, with $c/\ell = 0.1$, $t/c = 0.1$, $\tau_{cY}/\sigma_{fY} = 0.005$. Then, the transition overhang length H_t is given by $H_t = 0.1\ell$: an overhang of length 10% that of the sandwich panel span ℓ is sufficient to switch the collapse mode from Mode A to B. Furthermore, the enhancement in collapse load due to plastic bending of the face sheets above the load required to shear the core is about 20% for a small overhang $H \ll H_t$, and is about 40% for $H > H_t$. In much of the current literature on sandwich panels, a gross approximation is made by neglecting the contribution of the face sheets to the collapse load.

2.2. Finite element approach

In addition to upper bound plastic collapse analysis using beam theory, the finite element method has been used to calculate the load versus displacement response for selected geometries of sandwich panel. In the present study, the metallic foam constitutive law of Deshpande and Fleck [8] has been employed, with independently measured multi-axial data as input to the material description. Details of the foam properties are summarised in Section 3.1 below, and the constitutive law with finite element implementation [9] are described in Appendix A.

2.3. A collapse mechanism map for sandwich beams

It is assumed that the operative collapse mechanism for a sandwich beam is the one associated with the lowest collapse load. This can be shown graphically by plotting a non-dimensional measure of the upper bound collapse load $\bar{F} = F/(b\ell\sigma_{fY})$ on a diagram with the non-dimensional axes c/ℓ and t/c, for selected values of σ_{cY}/σ_{fY}. This method follows that pioneered by Gibson and Ashby [7] for polymeric foam cores and aluminium alloy face sheets.

An example of the collapse map is given in Fig. 4, with $\sigma_{cY}/\sigma_{fY} = 0.02$ and $s/\ell = 0.45$. It is assumed that the overhang H exceeds the transition value H_t so that core shear is by Mode B, as depicted in Fig. 3. The regimes of dominance for each collapse mechanism are marked: for example, it is clear that failure is by face yield for thin face sheets (small t/c) and for long beams (small c/ℓ). It is striking that the boundary between the core shear regime and the indentation regime has a large curvature, with core shear dominating at intermediate values of t/c. This is a consequence of the plastic hinge formation within the face sheets in the core shear collapse regime: the collapse load for core shear increases quadratically with increasing t/c due to the contribution from face sheet bending (see Eqs. (8) and (9)). Core shear dominates the map, for the values of parameters selected.

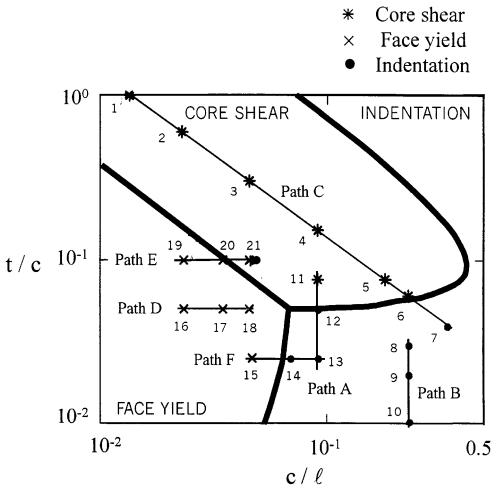

Fig. 4. Failure mechanism map of sandwich beams subjected to four-point bending with $\bar{s} = 0.45$ and $\bar{\sigma}_Y = 0.02$.

A similar map can be constructed for three-point bending (see, for example, Fig. 5 of Bart-Smith et al. [2] and Fig. 5 of McCormack et al. [3]). A comparison with the map of Fig. 4 reveals that the domain of face yield enlarges slightly and the regime of indentation increases greatly for three-point bending.

Now, some words of caution. Only plastic collapse mechanisms have been considered. Alternative failure modes are expected when the face sheets comprise monolithic ceramic or composite layers, and behave in an elastic-brittle manner. Then, collapse is dictated by fracture of the face sheets. This case has been analysed recently by Shuaeib and Soden [10] and Soden [11].

3. Experimental method

3.1. Materials and measured properties

Sandwich beams of width $b = 50\,\text{mm}$ were manufactured by bonding aluminium face-sheets to an aluminium alloy foam, and were then tested in four-point bend. The face-sheets were half-hard, commercial-purity aluminium sheets of thickness $t = 0.5$, 1.0, 1.5 and 3.0 mm. The foam core was a closed-cell aluminium-alloy foam, with trade-name Alporas; its relative density (density of the foam divided by the density of the cell wall material) was $\hat{\rho} = 11\%$, and the average cell size was 3 mm. The cell walls contain about 5% calcium in order to increase its viscosity in the molten state: the phase diagram for aluminium–calcium indicates a eutectic near this composition [12].

The aluminium face-sheets were degreased and abraded, and were then adhered to the foam core using Redux 322 epoxy adhesive on a nylon carrier mesh. The sandwich beams were air cured at 175°C for 1 h, and bonding was facilitated by imposing dead-loading with a nominal contact pressure of 0.01 MPa. The shear strength of the cured Redux 322 adhesive was taken to be 20 MPa,

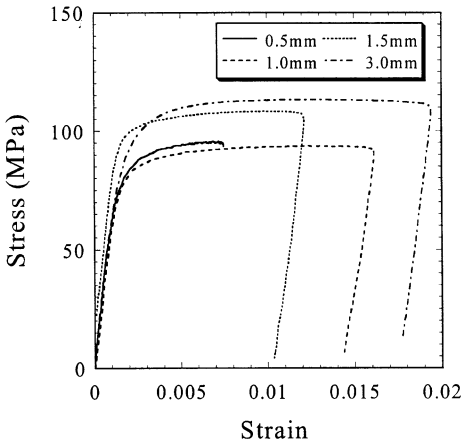

Fig. 5. Effect of thickness on the nominal stress–strain response in uniaxial tension, for the aluminium face sheets.

from Hexcel's data sheets[2]. (This strength is about one order of magnitude higher than that of the Alporas foam, and so no adhesive failure was observed.)

The mechanical properties of the face sheets and core were measured as follows. Tensile specimens of dogbone geometry were cut from the aluminium face sheets, with the longitudinal direction parallel to the rolling direction of the sheet. In order to measure the axial strain accurately, 120 Ω resistance strain gauges of gauge length 2 mm were oriented in the axial direction. The tensile nominal stress–strain curves for all four thicknesses are summarised in Fig. 5. The yield strength varies by up to 20% with thickness, and the tensile ductility lies in the range 0.7–2%. Checks revealed that the tensile stress–strain curves of the face sheets were not affected by the thermal cycle associated with bonding of the face sheets to the foam core. The Young's modulus of the face sheets was confirmed to be $E_f = 69$ GPa for all thicknesses, and the assumed Poisson ratio was $v_f = 0.3$.

The uniaxial tensile and compressive responses of the Alporas foam have already been reported by Harte et al. [13]. In brief, tension tests were performed on dogbone specimens of gauge length 100 mm and of cross-section 30 mm × 25 mm. Compression specimens were of cuboid geometry, measuring 50 mm × 50 mm × 75 mm. For both tension and compression, a clip gauge of length 20 mm was used to monitor the axial strain. Shear tests on Alporas foam were performed on blocks 100 mm × 20 mm × 20 mm using a double lap shear configuration as sketched in Fig. 6a, and a clip gauge to measure the relative motion of the outer plates with respect to the centre plate. Prior to performing the double lap shear tests, the Alporas foam shear specimens were adhered to steel grips using the Redux 322 epoxy adhesive.

Fig. 6b shows the tensile, compressive and shear stress–strain curves, plotted in terms of the overall effective stress $\hat{\sigma}$ and effective strain $\hat{\varepsilon}$, as defined in Appendix A. In Fig. 6b, $\hat{\sigma}$ and $\hat{\varepsilon}$ equal the uniaxial stress σ and strain ε, respectively, for tension and compression, while $\hat{\sigma} = 1.50\tau$ and $\hat{\varepsilon} = \gamma/1.50$ for a shear test of shear stress τ versus engineering shear strain γ since α as defined in

[2] Hexcel Publication RTC020 on Redux 322 adhesive (January 1997), Hexcel, Duxford, Cambridge, CB2 4QD, UK

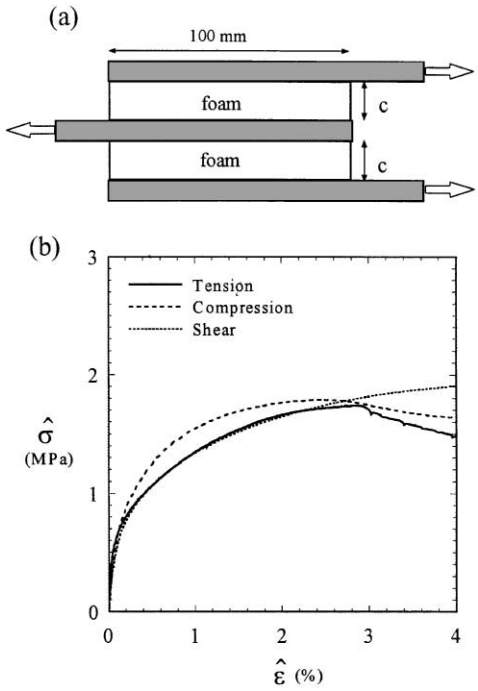

Fig. 6. (a) The geometry of the double lap shear specimens, for a core thickness c in the range 3–20 mm; (b) the stress versus strain responses of the Alporas foam ($\hat{\rho} = 11\%$) under uniaxial tension, compression, and simple shear.

Appendix A is 1.75 for the 11% dense Alporas. We note that the $\hat{\sigma}$ versus $\hat{\varepsilon}$ hardening response is relatively insensitive to type of test, in support of the Deshpande–Fleck model [8]. The Young's modulus of the Alporas foam is $E_c = 1.0\,\text{GPa}$, and the Poisson's ratio is $v_c = 0.15$.

Preliminary tests show that the tensile and compressive stress-strain responses are only mildly influenced by the specimen thickness, provided that the thicknesses exceeds 2–3 cell sizes. In contrast, the shear response is sensitive to the thickness of the specimen: the responses for a set of double lap shear specimens are given in Fig. 7, for a thickness c in the range 3–20 mm, and width fixed at 20 mm. A clear size effect is observed, with a stronger response displayed by specimens of diminishing thickness. The shear modulus G was found to be $G = 0.44\,\text{GPa}$, and was independent of thickness c to within material scatter. A similar size effect in shear has been reported by Andrews et al. [6] for the Alporas foam; they find additionally that the size effect disappears for thicknesses in excess of 20 mm.

3.2. Test method for sandwich beams

A 100 kN screw-driven test machine and four point bend rig were used to load the sandwich beams. The beams were loaded by cylindrical rollers of diameter 19 mm, and the inner rollers were displaced at a rate of $0.03\,\text{mm}\,\text{s}^{-1}$. Selected specimens were instrumented as follows to confirm the mechanism of collapse. A clip gauge was used to measure the change in height of beam directly under the inner rollers, and 120 Ω resistance strain gauges of length 2 mm were placed at mid-span

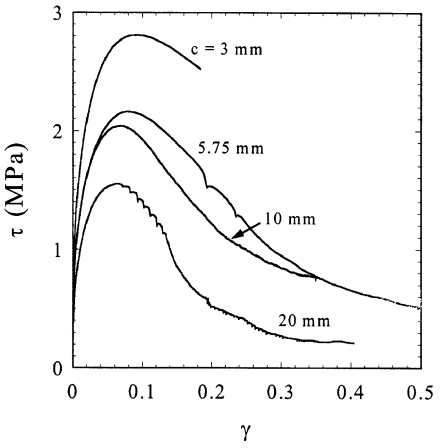

Fig. 7. Effect of specimen thickness c on the stress–strain curves of the Alporas foam in simple shear.

on both face sheets. An additional clip gauge was used to measure the relative sliding displacement of the face sheets, and thereby the average shear strain in the core.

4. Comparison between measured and simulated collapse responses

Tests were designed to determine the regimes of dominance of the various collapse modes. The geometries considered are summarised in Fig. 4, and in Table 1. The idea was to vary the specimen geometry along a number of design paths A–F in order to investigate each collapse mechanism. Additional tests were performed to determine the boundaries between the collapse modes. The results of this procedure are included in Fig. 4: the observed collapse modes are compared with predictions (4), (6) and (9) of limit load analysis. In general, the observed collapse mode agreed with the predictions. The exceptions is specimen number 21, which collapsed by a combination of core shear and indentation rather than the predicted mode of core shear. The discrepancy is not too surprising, since the geometry lies close to the boundary of the three collapse regimes. In passing, we note that Bart-Smith et al. [2] observed a similar behaviour in their study of Alporas-core sandwich beams in three-point bending.

In the remainder of this section, the measured and predicted collapse responses are reported for each collapse mode in turn.

4.1. Core shear

The load versus deflection of the inner rollers relative to the outer rollers was measured for a specimen (specimen number 25 of Table 1 and Fig. 4) of core thickness $c = 20$ mm, face-sheet thickness $t = 3$ mm, inner span $s = 100$ mm and outer span $\ell = 220$ mm. The response is shown in Fig. 8a for an overhang $H = 10$ mm; this overhang is sufficiently short compared to the transition value $H_t = 20$ mm for collapse to occur by Mode A; the contrasting case of core shear by Mode B is given in Fig. 8b, for a specimen of longer overhang, $H = 40$ mm, but with, otherwise, same

Table 1
Geometry of the four-point bend specimens

Specimen	Core thickness, c(mm)	Face thickness, t(mm)	Inner roller span, s(mm)	Outer roller span, ℓ(mm)	Overhang length, H(mm)
1	3.0	3.0	100	220	40
2	5.0	3.0	100	220	40
3	10.0	3.0	100	220	40
4	20.0	3.0	100	220	40
5	40.0	3.0	100	220	40
6	50.0	3.0	100	220	40
7	75.0	3.0	100	220	40
8	50.0	1.5	100	220	40
9	50.0	1.0	100	220	40
10	50.0	0.5	100	220	40
11	20.0	1.5	100	220	40
12	20.0	1.0	100	220	40
13	20.0	0.5	100	220	40
14	20.0	0.5	130	290	5
15	20.0	0.5	190	430	35
16	10.0	0.5	190	430	35
17	10.0	0.5	130	290	5
18	10.0	0.5	100	220	40
19	10.0	1.0	190	430	35
20	10.0	1.0	130	290	5
21	10.0	1.0	100	220	35
22	20.0	3.0	100	220	30
23	20.0	3.0	100	220	20
24	20.0	3.0	100	220	15
25	20.0	3.0	100	220	10
26	20.0	3.0	100	220	5

dimensions (specimen number 4 of Table 1). For both geometries, visual observations confirmed that the beam collapsed in shear, with plastic hinge formation in the face sheets. The load versus displacement curve shows a peak, with distributed microcracking within the core occurring beyond peak load. The peak load is accurately predicted by the limit load calculations (8) and (9), and by the finite element simulations. We note that the peak loads as measured by experiment and as calculated by finite element method slightly exceed the limit load values. We recall that the limit load calculations are based upon simple beam theory: this approximation does not provide a kinematically admissible velocity field for collapse of the sandwich beam, for finite values of face-sheet thickness t. Thus, the limit load calculation is not a strict upper bound. We note in passing that the predicted elastic stiffness of the beam by the beam formula (1) and by the finite element calculations are in agreement with the measured stiffness, for both beams shown in Fig. 8.

A switch in the shear response from Mode A to B has been explored by performing a series of experiments (and accompanying calculations) for a beam of core depth $c = 20\,\text{mm}$, face-sheet thickness $t = 3\,\text{mm}$, inner span $s = 100\,\text{mm}$, outer span $\ell = 220\,\text{mm}$, and overhang H in the range

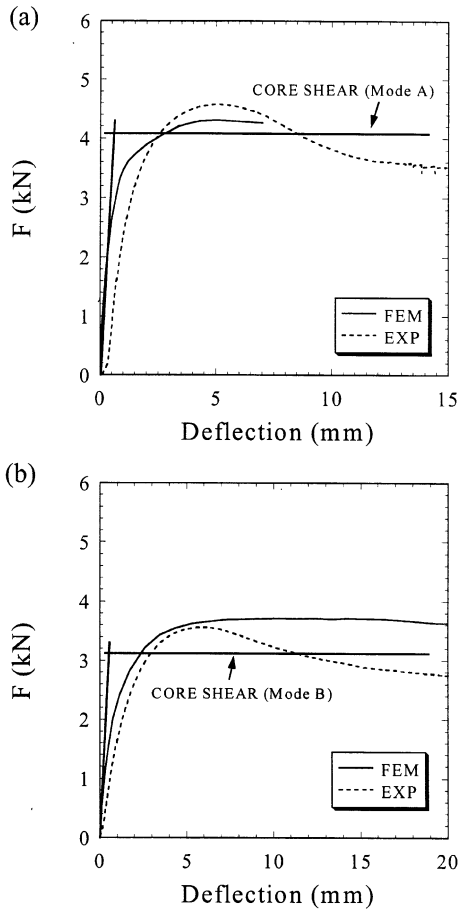

Fig. 8. Measured (EXP) and predicted (FEM) load versus displacement responses of sandwich beams for collapse by core shear. The beam theory predictions of stiffness (1) and strength (8) and (9) are included. (a) Core shear in Mode A, with $c = 20\,\text{mm}$, $t = 3\,\text{mm}$, $s = 100\,\text{mm}$, $\ell = 220\,\text{mm}$, and $H = 10\,\text{mm}$ (specimen number 25); (b) core shear in Mode B, with $c = 20\,\text{mm}$, $t = 3\,\text{mm}$, $s = 100\,\text{mm}$, $\ell = 220\,\text{mm}$, and $H = 40\,\text{mm}$ (specimen number 4).

5–40 mm. The associated peak loads are summarised in Fig. 9. Although the finite element and limit load predictions lay somewhat below the observed peak loads, the transition in mode occurs at $H = 20\,\text{mm}$ by all three methods. Visual observations of the deformed profile of the beams confirmed the transition in collapse mode with increasing H.

The limit load formulae (8) and (9) suggest that the peak load increases linearly with the core thickness c. To explore this, beams of geometry defined by path C of Fig. 4 were tested, and the associated peak loads are recorded in Fig. 10. The range of core thickness (3–50 mm) is sufficiently wide for a log–log plot to be required to display the data. Good agreement is noted between the limit load predictions, the finite element predictions and the measured collapse loads provided the shear strengths of the core in the predictions are the measured values for that thickness of core, as detailed in Section 3.1.

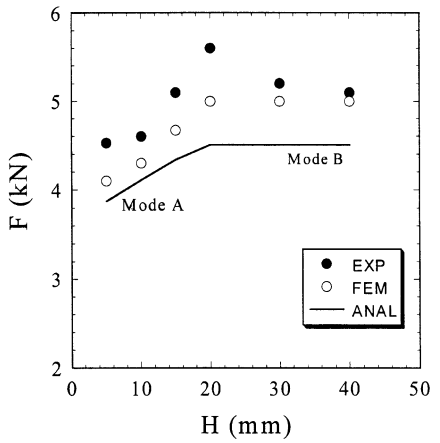

Fig. 9. Effect of the overhang length H on the peak load of sandwich beams for collapse by core shear. Values are plotted for the measured strength (EXP), the predictions of finite element analysis (FEM) and limit load analysis (ANAL).

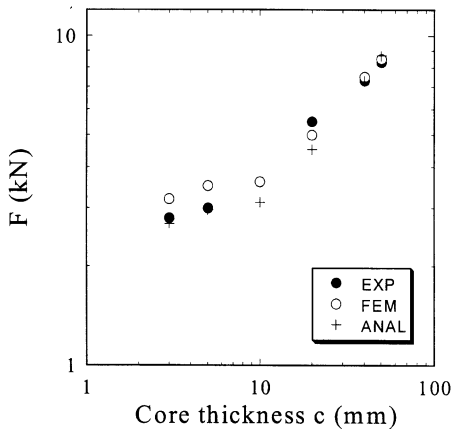

Fig. 10. Effect of the core thickness c on the peak load for collapse by core shear (specimen geometries coincide with path C in Fig. 4).

4.2. Face yield

Face yield is the dominant collapse mechanism when the span ℓ is large and the face-sheet thickness t is small in relation to the core thickness c. A typical collapse response is shown in Fig. 11 for the case $c = 10\,\text{mm}$, $t = 0.5\,\text{mm}$, $s = 100\,\text{mm}$, $\ell = 220\,\text{mm}$ and $H = 40\,\text{mm}$ (specimen number 18 in Fig. 4 and Table 1). The load increases monotonically with deflection until the face sheet in tension fails at a surface strain equal to its ductility (0.7%). The post-yield hardening behaviour is due to finite rotation effects. Finite element predictions are included in Fig. 11, and are based on the following description of the foam. The constitutive law for the core was calibrated against the shear stress–strain curve for an independent double-lap shear test on a specimen of thickness $c = 10\,\text{mm}$.

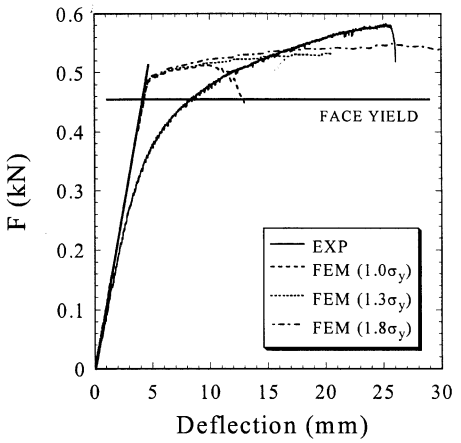

Fig. 11. Measured (EXP) and predicted (FEM) load versus displacement curves for a sandwich beam, for collapse by face yield. Additional finite element predictions are given for the core strength elevated by 30 and 80%. The beam theory predictions of stiffness (1) and strength (4) are also included. The geometry is $c = 10\,\text{mm}$, $t = 0.5\,\text{mm}$, $s = 100\,\text{mm}$, $\ell = 220\,\text{mm}$, and $H = 40\,\text{mm}$ (specimen number 18).

Recall that the shear response and the uniaxial tension and compression responses can be brought into alignment using the normalisation adopted within the Deshpande–Fleck model [8] (see Fig. 6). Surprisingly, the finite element calculations for the sandwich beam suggested that collapse was by core indentation rather than by face yield. Numerical experiments revealed that the indentation mode was switched off upon increasing the core strength by 30% or more, as shown in Fig. 11. No explanation has been forthcoming for this discrepancy in failure mode: visual inspection of the sandwich beam revealed no evidence of plastic indentation. However, the peak load as predicted by the finite element method, with the unelevated stress–strain response for the foam core, is in reasonable agreement with the observed collapse strength.

The limit load prediction (4) suggests that the collapse load increases linearly with $(\ell - s)^{-1}$. To verify this, a series of tests were performed with geometry defined by path D of Fig. 4, and the associated peak load for these geometries are shown in Fig. 12. The measurements confirm that the peak load increases with $(\ell - s)^{-1}$, with formula (4) in excellent agreement with the measured values. Finite element calculations were also performed, and were based upon the measured stress-strain shear response of the foam (for a core thickness $c = 10\,\text{mm}$). Again, the finite element method gives indentation rather than face yield as the dominant failure load, although the predicted peak loads are in good agreement with the observed values.

4.3. Indentation

The mechanism map Fig. 4 suggests that a sandwich beam collapses by indentation at sufficiently large values of core thickness c in relation to span ℓ. A highly instrumented test was performed to explore the indentation collapse mode, by taking $c = 20\,\text{mm}$, $s = 100\,\text{mm}$, $\ell = 220\,\text{mm}$ and $t = 0.5\,\text{mm}$ (specimen number 13 in Fig. 4 and Table 1). The measured load versus roller displacement response is shown in Fig. 13a for two nominally identical experiments 1 and 2.

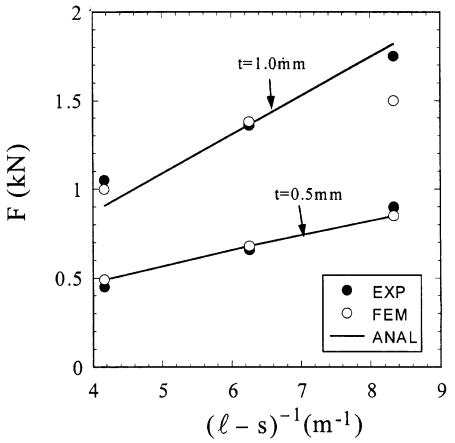

Fig. 12. Effect of the distance between inner and outer rollers on the peak load for collapse by face yield (specimen geometries are along path E in Fig. 4). Values are plotted for the measured strength (EXP), the predictions of finite element analysis (FEM) and limit load analysis (ANAL).

The predicted collapse responses by limit load analysis and by the finite element method are included in the figure. The measured peak load shows a variation of about 20% between the two tests, due to scatter in foam strength. In contrast, the limit load analysis and finite element predictions give almost identical peak loads, which are about 40% below the mean value of measured peak load. The observed collapse mode and the mode predicted by the finite element method were consistent with the indentation mode sketched in Fig. 2. It appears that the observed collapse response is significantly stronger than that predicted by the theoretical methods, despite the fact that the constitutive law for the foam core was calibrated against independent shear test data (from a double lap shear test, with foam of thickness 20 mm). It is conjectured that the discrepancy is associated with the fact that a boundary layer of strengthened foam exists adjacent to the face-sheets. The development of a theoretical framework to analyse this phenomenon is beyond the scope of the present study. As an initial attempt to gain insight into the discrepancy between theory and experiment, additional finite element calculations were performed using a foam core of strength elevated by 50 and 100% throughout the thickness of the core. The associated predictions of collapse response are given in Fig. 13a; it is concluded that a strength elevation of 100% is required in order for the predicted collapse response to be in reasonable agreement with the observed response. It is recalled from the shear strength measurements for thin sandwich specimens in Fig. 7 that boundary layer effects can give rise to strength elevations within the foam by a factor of up to 2.

In order to gain additional insight into the indentation collapse mode, test 1 was performed with the following instrumentation:

Type (*i*): a through-thickness clip gauge was fastened between the upper and lower face sheets, directly beneath one of the inner rollers, in order to measure the relative approach of the face sheets.

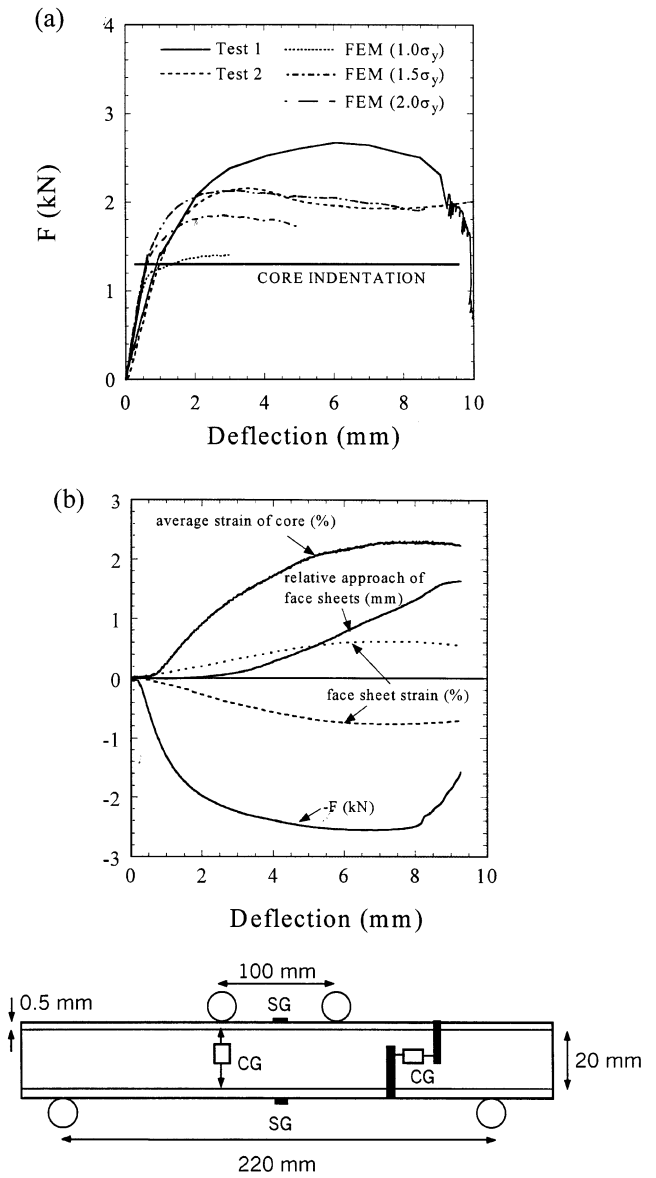

Fig. 13. (a) Measured (EXP) and predicted (FEM) load versus displacement curves of a sandwich beam failed by indentation, with $c = 20\,\text{mm}$, $t = 0.5\,\text{mm}$, $s = 100\,\text{mm}$, $\ell = 220\,\text{mm}$, and $H = 40\,\text{mm}$ (specimen number 13). Additional finite element predictions are given for the core strength elevated by 50 and 100%; (b) measured collapse response for Test 1, using additional clip gauges and strain gauges. The specimen geometry is sketched, with the locations of the strain gauges (SG) and clip gauges (CG) marked.

Type (*ii*): axial strain gauges were adhered to the top and bottom face sheets, mid-way between the two inner rollers, in order to determine the degree of face-yield in bending.

Type (*iii*): a transverse clip gauge was located between an inner and outer roller support in order to measure the shear sliding displacement of the top relative to the bottom face sheet. This gauge

was used to measure the average shear strain within the core, in order to check for collapse by core shear.

Fig. 13b shows the measured load and output from the above three gauges for test 1, plotted against the relative displacement of the upper and lower rollers. We deduce from the correlation between the indentation-measuring clip gauge of type (i) and the load response that the collapse mechanism is indentation. The level of shear strain in the core attains a maximum value of 2% which exceeds the shear yield strain of 0.5%, but is much less than the failure strain in shear of about 8%. It is inferred that the collapse mode of core shear is inoperative. Face yield also appears to play only a minor role for this geometry: the axial strain of the face sheets attains a peak value of about 0.6%, which is somewhat larger than the yield strain of 0.2% for the face-sheets but lower than the tensile failure strain of 0.7%. Visual observations of the face-sheets confirmed that the face-sheets do not fracture.

Formula (6) suggests that the indentation collapse load increases (linearly) with the face-sheet thickness. The measured collapse load for geometries along path A of Fig. 4 is plotted against thickness t in Fig. 14, with $c = 20\,\text{mm}$ and $\ell = 220\,\text{mm}$. The predictions by limit load analysis and the finite element method, each calibrated by the independently measured shear response for the foam (of thickness $c = 20\,\text{mm}$), are included in Fig. 14. We note that the finite element and limit load analysis are in good agreement, but the measured collapse load is 70% above the predictions for the choice $t = 0.5\,\text{mm}$; this case has already been discussed above and reported in Figs. 13a and b. Close agreement between the measured and predicted collapse loads was observed, however, for the choice $t = 1\,\text{mm}$; in this case, collapse was by a combination of core shear and indentation, consistent with the fact that this geometry lies adjacent to the boundary with the core shear regime (see Fig. 4). Thus, an interaction of modes occurred, with a reduced net collapse load.

In addition to the indentation mode depicted in Fig. 2, an alternative indentation mode was observed at large values of c/ℓ. Then, indentation was by local stretching of the face-sheets beneath the inner and outer rollers, with indentation of the underlying foam core; this mode is sketched as

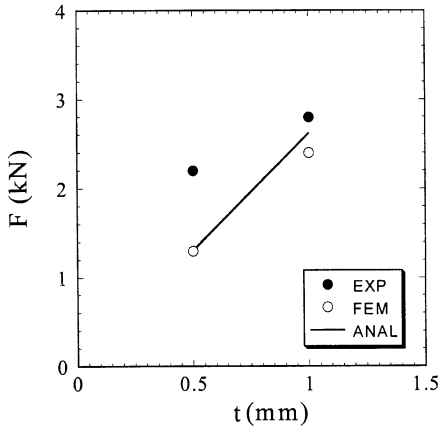

Fig. 14. Effect of face sheet thickness t on the peak load of sandwich beams for collapse by indentation (specimen geometries are along path A in Fig. 4). Values are plotted for the measured strength (EXP), the predictions of finite element analysis (FEM) and limit load analysis (ANAL).

an insert to Fig. 15. The measured collapse response for this mode is shown in Fig. 15, for the choice $t = 1$ mm, $c = 50$ mm, $s = 100$ mm and $\ell = 220$ mm: the load increases monotonically with deflections, and no limit load is achieved by this mode. The finite element predictions are in excellent agreement with the observed response, but no limit load analysis is appropriate. The effect of face sheet thickness t on the collapse response is summarised in Fig. 16, for geometries specified along Path B of Fig. 4. The back-extrapolated collapse load F_{BE} is plotted against t in Fig. 16, by locating the intersect between the initial elastic response and the post-yield response. It is noted that F_{BE} increases with t, and good agreement is achieved between finite element predictions and the observed responses.

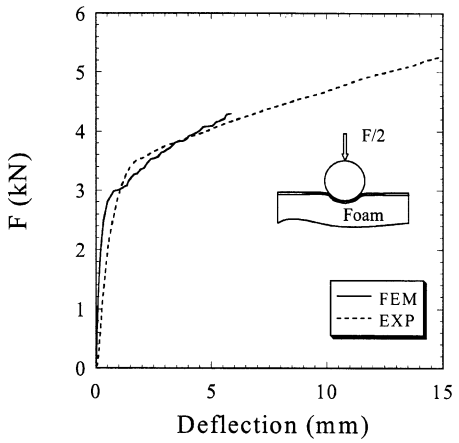

Fig. 15. Measured (EXP) and predicted (FEM) load versus displacement curves of a sandwich beam for collapse by indentation. The geometry is $c = 50$ mm, $t = 1$ mm, $s = 100$ mm, $\ell = 220$ mm, and $H = 40$ mm (specimen number 9).

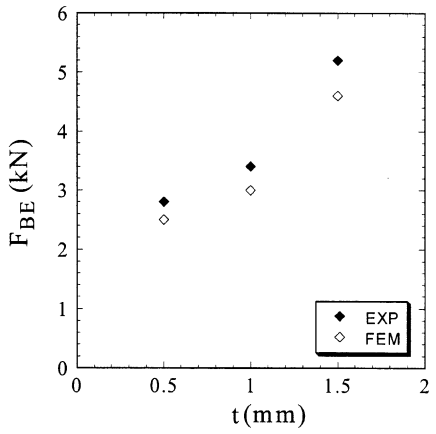

Fig. 16. Effect of face sheet thickness t on the back-extrapolated F_{BE} yield load of sandwich beams, for collapse by indentation (specimen geometry along path B in Fig. 4). Values are plotted for the measured strength (EXP), and for the predictions of finite element analysis (FEM).

5. Minimum weight design

The design of sandwich beams can be optimised to minimise weight, cost or some other objective function, against constraints such as a given collapse strength, beam stiffness or some other structural index. Here, we shall assume that the optimal sandwich beam is the one of minimum weight M for a given collapse load F. We begin by redefining the geometry, collapse load and beam weight in non-dimensional terms. The non-dimensional face sheet thickness $\bar{t}$, core thickness $\bar{c}$ and inner span $\bar{s}$ are defined by

$$\bar{t} \equiv t/\ell, \quad \bar{c} \equiv c/\ell \quad \text{and} \quad \bar{s} \equiv s/\ell, \tag{11}$$

respectively. The ratio of strength of core to face sheet is

$$\bar{\sigma}_Y \equiv \sigma_{cY}/\sigma_{fY} \tag{12}$$

and the density ratio $\bar{\rho}$ is

$$\bar{\rho} \equiv \rho_c/\rho_f, \tag{13}$$

where ρ_c and ρ_f are the densities of the core and face sheet, respectively. The non-dimensional weight of the sandwich beam $\bar{M}$ is related to the weight M of the beam by

$$\bar{M} \equiv \frac{M}{\rho_f b \ell^2} = 2\bar{t} + \bar{c}\bar{\rho} \tag{14}$$

and the non-dimensional *structural load index* $\bar{F}$ is

$$\bar{F} \equiv \frac{F}{b\ell\sigma_{fY}} \tag{15}$$

in terms of the collapse load F.

By virtue of Eq. (15), expressions for $\bar{F}$ follow from Eqs. (4), (5) and (9) as

$$\bar{F}_{FY} = \frac{4\bar{t}(\bar{c}+\bar{t})}{1-\bar{s}} + \frac{\bar{c}^2}{1-\bar{s}}\bar{\sigma}_Y \tag{16}$$

for face yield,

$$\bar{F}_I = 4\bar{t}\sqrt{\bar{\sigma}_Y} \tag{17}$$

for indentation, and

$$\bar{F}_B = \frac{4\bar{t}^2}{1-\bar{s}} + 2\bar{c}\bar{\sigma}_Y \frac{\tau_{cY}}{\sigma_{cY}} \tag{18}$$

for core shear in Mode B.

The optimal weight design is obtained by selecting the beam geometry $(\bar{t}, \bar{c})$ which minimises the weight $\bar{M}$ for a given structural load index $\bar{F}$. For this purpose, it is instructive to plot the contours

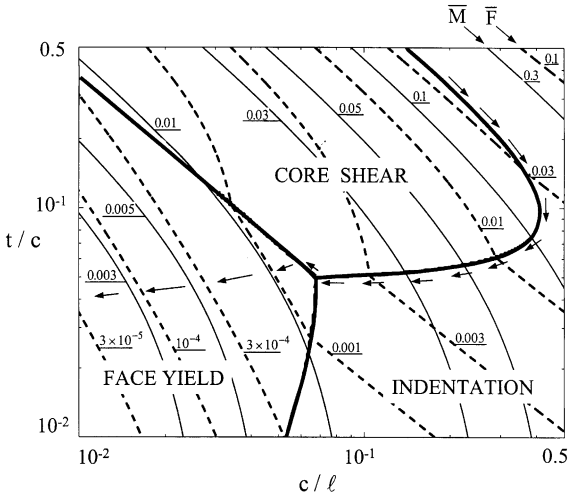

Fig. 17. Collapse mechanism map for beam in four-point bending, for the case $\bar{s} = 0.45$, $\bar{\sigma}_Y = 0.02$ and $\bar{\rho} = 0.1$. Contours of the dimensionless weight $\bar{M}$ and the structural load index $\bar{F}$ have been added. The arrows trace the path of the minimum weight designs with diminishing $\bar{F}$.

of $\bar{M}$ and $\bar{F}$ on the collapse mechanism map, as shown in Fig. 17 for the case $\bar{\sigma}_Y = 0.02$, $\bar{s} = 0.45$ and $\bar{\rho} = 0.1$. The contours of both $\bar{F}$ and $\bar{M}$ increase along the leading diagonal of the map, with increasing $\bar{c} = c/\ell$ and $t/c = \bar{t}/\bar{c}$. We further note from Fig. 17 that the minimum weight design is achieved within the face yield regime for low values of $\bar{F}$ and at the boundary between the core shear and indentation regimes for high values of $\bar{F}$. For intermediate values of $\bar{F}$ (that is, $10^4\bar{F} \approx 20$) the minimum weight design occurs at the boundary between the face yield and core shear regimes, for the chosen values of $\bar{\sigma}_Y$, $\bar{s}$, and $\bar{\rho}$. The arrows shown in Fig. 17 give the path of minimum weight design with diminishing $\bar{F}$.

An analytic expression can be obtained for the minimum weight $\bar{M}_{\min}$ at low values of $\bar{F}$; then, collapse is by face yield, and minimisation of $\bar{M}$ with respect to $(\bar{t}, \bar{c})$ at fixed $\bar{F}$ gives

$$\bar{M}_{\min} = K\sqrt{\bar{F}}, \tag{19}$$

where

$$K = (2\bar{\rho} - \bar{\rho}^2 - \bar{\sigma})\left(\frac{1-\bar{s}}{(1-\bar{\sigma}_Y)^2 - (1-\bar{\sigma}_Y)(1-\bar{\rho})^2}\right)^{1/2}. \tag{20}$$

Explicit expressions for the minimum weight designs along the boundaries of the collapse map can be obtained in a straightforward manner; however such expressions are lengthy and are omitted here for the sake of brevity. The minimum weight $\bar{M}_{\min}$ is plotted as a function of $\bar{F}$ in Fig. 18a, for the above case $\bar{s} = 0.45$ (with $\bar{\sigma}_Y = 0.02$ and $\bar{\rho} = 0.1$). The associated optimal geometry $(\bar{t}, \bar{c})$ is included in the figure and, as expected, $\bar{t}$ and $\bar{c}$ increase with load level $\bar{F}$. It is instructive to explore the effect of the span $\bar{s}$ on the minimum weight design $\bar{M}_{\min}$, as shown in Fig. 18b. Results

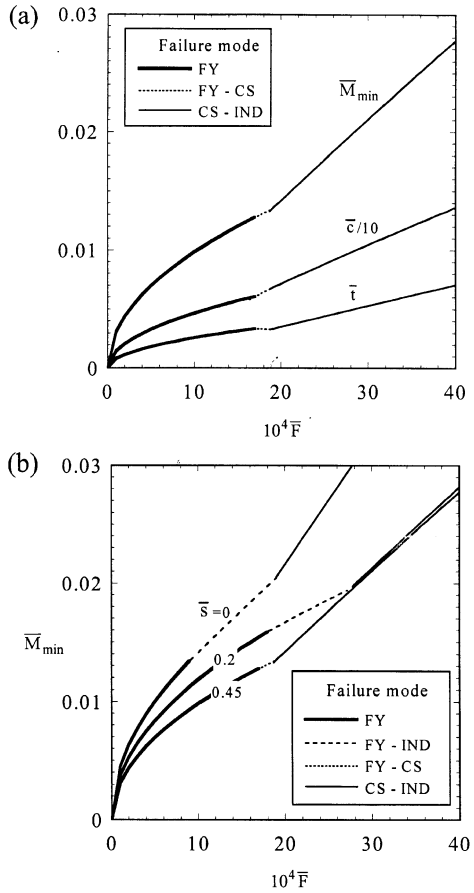

Fig. 18. Minimum weight designs of sandwich beams with $\bar{\sigma}_Y = 0.02$ and $\bar{\rho} = 0.1$. Depending upon the assumed value of $\bar{F}$, collapse is by face yield (FY), by combined face yield and core shear (FY–CS), by combined face yield and indentation (FY–IND) or by combined core shear and indentation (CS–IND). (a) Details of the optimal design for the case $\bar{s} = 0.045$; (b) effect of the inner span $\bar{s}$ upon the minimum weight design.

are given for $\bar{s} = 0.45$ and 0.2, and for the case of 3-point bending (denoted by $\bar{s} = 0$). For the case of three-point bending, the face-yield collapse load is given by (4) with $\bar{s} = 0$; for indentation, the collapse load is half the value given by (6) since only a single inner roller is present. For core shear, the loads for collapse modes A and B are modifications to Eqs. (8) and (9), respectively, with explicit formulae given by Ashby et al. [1]. It is noted from Fig. 18b that face yield dominates at low values of $\bar{F}$, whereas collapse is by simultaneous core shear and indentation at large values of $\bar{F}$, for all values of inner span $\bar{s}$. For intermediate values of $\bar{F}(\approx 20\times 10^{-4})$ collapse switches from simultaneous face yield and core shear at $\bar{s} = 0.45$ to simultaneous face yield and indentation at lower values of $\bar{s}$. For a given value of structural load index $\bar{F}$, the minimum weight beam in three-point bend is about twice that of the beam in four-point bend (with $\bar{s} = 0.45$).

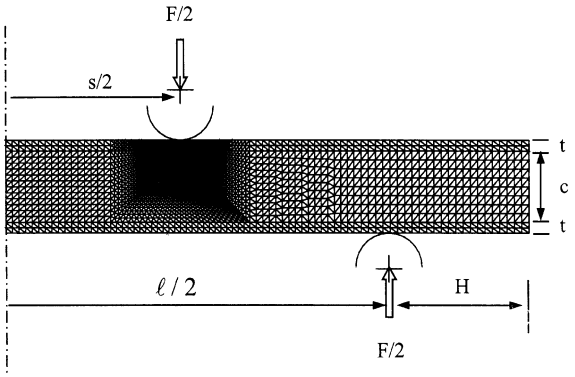

Fig. 19.

6. Concluding remarks

This study has shown that the analytic formulae given by limit load analysis are in good agreement with the predictions by more refined finite element calculations and the measured collapse strengths. These formulae can be used directly in minimum weight design and reveal that the optimal sandwich beam lies at the boundary of competing collapse modes, for high values of structural load index; at low values of load index, the optimal design collapses by face yield for both three- and four-point bend loading. There remain some subtleties, however, in the comparison of the predicted and the observed collapse responses. For collapse by core shear, a core thickness effect needs to be taken into account in order to obtain accurate predictions both by limit load analysis and by the finite element method: thin cores are stronger in shear than thick cores. For the case of indentation, the measured collapse load exceeds the predicted value (by either theoretical method) by up to 50%; it is thought that the discrepancy is due to the presence of a boundary layer within the foam core near the bonded interface with the face sheets. Such effects could be modelled using a strain gradient theory of plasticity, for example, the Fleck and Hutchinson theory [14].

Acknowledgements

This work was supported by the EPSRC (U.K.) and by the DARPA/ONR (U.S.A.) MURI program on Ultralight Metallic Structures (No. N00014-1-96-1028). The authors are grateful for helpful discussions with Prof. M.F. Ashby.

Appendix A

A.1. Constitutive model of metallic foams

In the present finite element study, the sandwich core made of Alporas foams is treated as homogeneous solid. Its constitutive behaviour is modelled by the phenomenological constitutive

model developed by Deshpande and Fleck [8]. The model has been implemented into the commercial finite element code ABAQUS through the user subroutine interface UMAT [9] and is used in this paper to characterise the behaviour of the sandwich core.

In the constitutive model developed by Deshpande and Fleck [8], the yield function Φ is assumed to be

$$\Phi = \hat{\sigma} - Y = 0, \tag{A.1}$$

where Y is the uniaxial yield strength and $\hat{\sigma}$ is the effective stress, defined by

$$\hat{\sigma}^2 = \frac{1}{1 + (\alpha/3)^2}(\sigma_e^2 + \alpha^2\sigma_m^2), \tag{A.2}$$

where α defines the aspect ratio of the elliptical yield surface in the Mises stress σ_e and mean stress σ_m space. Note that for the case $\alpha = 0$, the effective stress $\hat{\sigma}$ reduces to σ_e and the J_2 flow theory is recovered. According to Deshpande and Fleck [8], α is related to the plastic Poisson's ratio v^p by

$$\alpha = 3\left(\frac{1/2 - v^p}{1 + v^p}\right)^{1/2} \tag{A.3}$$

Consequently, instead of probing the shape of the initial yield surface and its subsequent evolution from complicated multi-axial tests, it appears from Eq. (A.3) that the yield surface can be estimated by simply measuring v^p in a uniaxial test. For lightweight Alporas foams, the plastic Poisson's ratio is approximately zero ($v_p \approx 0$) and hence, from (A.3), $\alpha \approx 2.12$ [8].

For simplicity, isotropic hardening is assumed below, i.e., the yield surface grows in a geometrically self-similar manner with strain. Limited data on the yield surface of Alporas foams [8] suggests that this approximation may be appropriate. To model the post-yield behaviour, an effective plastic strain rate $\dot{\hat{\varepsilon}}$, the work rate conjugate to $\hat{\sigma}$, is introduced as

$$\begin{aligned} \dot{\hat{\varepsilon}}^2 &= [1 + (\alpha/3)^2](\dot{\varepsilon}_e^2 + \dot{\varepsilon}_m^2/\alpha^2), \\ \dot{\varepsilon}_e^2 &= (2/3)\dot{\varepsilon}_{ij}^p\dot{\varepsilon}_{ij}^p, \quad \dot{\varepsilon}_m = \dot{\varepsilon}_{ii}^p, \end{aligned} \tag{A.4}$$

where $\dot{\varepsilon}_{ij}^p$ is the plastic strain rate, $i,j = 1, 2, 3$, and the convention of summation over repeated indices applies. With the assumption of normality, the plastic strain-rate is given by

$$\begin{aligned} \dot{\varepsilon}_{ij}^p &= \dot{\hat{\varepsilon}}\frac{\partial\Phi}{\partial\sigma_{ij}} \\ &= \frac{\dot{\hat{\varepsilon}}}{1 + (\alpha/3)^2}\left(\frac{3}{2}\frac{s_{ij}}{\hat{\sigma}} + \frac{\alpha^2}{3}\delta_{ij}\frac{\sigma_m}{\hat{\sigma}}\right), \end{aligned} \tag{A.5}$$

where $s_{ij} = \sigma_{ij} - \sigma_m\delta_{ij}$ is the deviatoric stress, δ_{ij} is the Kronecker delta, and the effective strain rate is connected to the effective stress rate by

$$\dot{\hat{\varepsilon}} = \frac{\dot{\hat{\sigma}}}{H(\hat{\sigma})}. \tag{A.6}$$

Here, $H(\hat{\sigma})$ is the tangent of the uniaxial true stress versus logarithmic plastic strain curve at stress level $\sigma = \hat{\sigma}$.

A.2. The finite element model

Due to symmetry, only half-length of the sandwich panel subjected to four point bending is modelled. Eight-noded two-dimensional elements are used to discrete the sandwich core and the aluminium skins. The contact interaction between the panel and the rollers is modelled by the contact surfaces provided by the ABAQUS. The prescribed displacement conditions are applied to the rollers to impose the load. Before doing further calculations, mesh sensitivity study has been performed to ensure that the finite element meshes are fine enough to give satisfactory results. A typical mesh is illustrated in Fig. 19.

In the finite element model, the aluminium skins are modelled by J2 flow theory and the sandwich core is represented by the constitutive model of Deshpande and Fleck [8]. As previously mentioned, experiments show that the uniaxial stress–strain curves of the aluminium skins and the shear stress–strain curves of the Alporas foam depend upon the thickness of the specimens. Thus, the constitutive models for both the aluminium skins and the Alporas foams were calibrated against corresponding data from specimens of the same thickness.

References

[1] Ashby MF, Evans AG, Fleck NA, Gibson LJ, Hutchinson JW, Wadley HNC. Metal foam: a design guide. Oxford: Butterworth Heinemann, 2000.
[2] Bart-Smith H, Hutchinson JW, Evans AG. Measurement and analysis of the structural performance of cellular metal sandwich construction. International Journal of Mechanical Sciences 2000; in press.
[3] McCormack TM, Miller R, Kesler O, Gibson LJ. Failure of sandwich beams with metallic foam cores. International Journal of Mechanical Sciences 2000; submitted for publication.
[4] Allen HG. Analysis and design of structural sandwich panels. Oxford: Pergamon Press, 1969.
[5] Wilsea M, Johnson KL, Ashby MF. Indentation of foamed plastics. International Journal of Mechanical Sciences 1975;17:457–60.
[6] Andrews EH, Gioux G, Onck P, Gibson LJ. Size effects in ductile cellular solids, Part II: experimental results. International Journal of Mechanical Sciences 2001;43:701–13.
[7] Gibson LJ, Ashby MF. Cellular solids, structure and properties, 2nd ed. Cambridge: Cambridge University Press, 1997.
[8] Deshpande VS, Fleck NA. Isotropic constitutive models for metallic foams. Journal of the Mechanics and Physics of Solids 2000;48:1253–83.
[9] Chen C. Manual for a UMAT user subroutine. Cambridge University Engineering Department Report, CUED/C-MICROMECHANICS/TR.4, 1998.
[10] Shuaeib FM, Soden PD. Indentation failure of composite sandwich beams. Composite Science and Technology 1997;57:1249–59.
[11] Soden PD. Indentation of composite sandwich beams. Journal of Strain Analysis 1996;31(5):353–60.
[12] Miyoshi T, Itoh M, Akiyama S, Kitahara A. Aluminium foam, 'Alporas': the production process, properties and applications. In: Banhart J, Ashby MF, Fleck NA, editors. Proceedings of Metal Foams and Porous Metal Structures. Cambridge, MA: MIT Press, 1999. p. 125–32.
[13] Harte AM, Fleck NA, Ashby MF. Fatigue failure of an open cell and a closed cell aluminium alloy foam. Acta Materialia 1999;47:2511–24.
[14] Fleck NA, Hutchinson JW. Strain gradient plasticity. In: Hutchinson JW, Wu TY, editors. Advances in applied mechanics., Vol. 33. New York: Academic Press, 1997. p. 295–361.